Development of Energetic and Enzymatic Limitations on Microbial Carbon Cycling in Upland Soils

Hannah R. Naughton,[1] Marco Keiluweit,[2] Malak M. Tfaily,[3] James J. Dynes,[4] Tom Regier,[4] Scott Fendorf[1*]

1. Earth System Science Department, Stanford University, Stanford, CA 94305

2. Stockbridge School of Agriculture, University of Massachusetts, Amherst, MA 01003

3. Department of Environmental Sciences, The University of Arizona, Tucson, AZ 85719

4. Canadian Light Source Inc., Saskatoon, SK, Canada

* Corresponding author: fendorf@stanford.edu

Keywords: soil organic carbon preservation, soil redox chemistry, extracellular oxidative enzymes, microbial carbon utilization

Acknowledgements: This research was supported by the U.S. National Science Foundation (Graduate Research Fellowship to H.R.N) and the U.S. Department of Energy Office of Biological and Environmental Research, Subsurface Biogeochemistry Program (Award Number DE-SC0016544). Parts of the research used in this paper were supported by U.S. Department of Energy and the Canadian Light Source, a national research facility of the University of Saskatchewan, which is supported by the Canada Foundation for Innovation (CFI), the Natural Sciences and Engineering Research Council (NSERC), the National Research Council (NRC), the Canadian Institutes of Health Research (CIHR), the Government of Saskatchewan, and the University of Saskatchewan. Important thanks go to D. Nakoa Farrant, H. Tang, D. Turner and G. Li for their assistance running the experiment and performing instrumental analysis.

Abstract

Soil organic carbon (SOC) constitutes an important stock in the global carbon cycle that is vulnerable to transformation and loss due to land use and climate change. Anaerobic conditions protect SOC from microbial degradation by hindering respiration through poor energetics and inhibition of extracellular oxidative enzymes that convert polymeric substrates into respirable organic compounds. Given growing evidence of prevalent anaerobic microsites in formally upland soils, we designed an experiment testing the development of dissolved organic carbon (DOC) signatures of energetic and enzymatic limitations on microbial carbon utilization across soil aggregates. Reactors comprised a soil column "aggregate" underlying an advective "macropore" channel. Soils received downward diffusive inputs of aerated groundwater media with added nitrate, sulfate, or no amendment – where native ferrihydrite served as dominant anaerobic terminal electron acceptor (TEA) – to contrast energetic regimes' control of DOC cycling along a diffusive oxygen gradient. After forty days, added nitrate resulted in highest bulk respiration and DOC production while sulfate did not differ from the control. Nominal oxidation state of carbon (NOSC) was higher (more favorable) with added TEAs at soil surfaces and decreased with depth, while the control NOSC remained lower and constant with depth. DOC generally increased with depth, which with NOSC values indicates joint electron-donor and acceptor control over respiration thermodynamics. Of all organic compound classes, only phenolics' relative abundance step-increased between 0 and 0.5 cm depth, coinciding with loss of oxygen and inhibition of oxidative enzymes. Upland soils rapidly preserve SOC via energetic and enzymatic mechanisms under anaerobiosis that aeration would expose for oxidation.

Introduction

Soils hold more dynamic carbon than the atmosphere and Earth's biota combined (Jackson et al. 2017). Between 60 and 75% of the land surface experiences anthropogenic alterations such as tilling, logging, nutrient or pesticide application, and cropping or ranging (Ellis 2011), all processes that may alter soil organic carbon (SOC) storage. Furthermore, long-term trends in global temperatures, atmospheric carbon and precipitation patterns will alter the stability of stored carbon (Fierer et al. 2003; Falloon et al. 2007; Groenigen et al. 2014; Crowther et al. 2016). Given the host of anthropogenic and climatic factors impacting soils, projecting and managing carbon storage will rely on accurate quantification and a clear understanding of the mechanisms leading to the preservation and release of SOC.

Unfortunately, despite a significant number and diversity of carbon cycle models, processed-based models projecting the fate of soil carbon remain a goal (Jackson et al. 2017). Earth System Models do not agree on the magnitude of changes in SOC stocks and atmospheric fluxes going into the future (Arora et al. 2013; Luo et al. 2015). This disagreement is attributed predominantly to missing and unlinked soil processes (Zhou et al. 2012; Schmidt 2012; Wieder et al. 2013; Doetterl et al. 2015; Lehmann and Kleber 2015) that include microbial community dynamics, joint transformations of minerals and carbon, and environmental factors.

Implicated by each of these suggested factors impacting SOC cycling lies a common yet unmentioned theme: energy. Soil factors such as water saturation state (moisture level), soil structure, and chemistry influence electron acceptor availability and thus energy available for microbial respiration. The concept of metabolic energy controlling microbial carbon cycling is not novel (Sørensen 1982; Lovley and Phillips 1988; Nealson and Myers 1992; Canfield et al. 1993; Thamdrup 2000; Davidson et al. 2012) and has in the past two decades been expanded to

represent the energetics of organic electron donors (Jin and Bethke 2003; LaRowe and Van Cappellen 2011; LaRowe et al. 2012; Keiluweit et al. 2016, 2017; Boye et al. 2017) and enzymatic limitations on depolymerization (Sinsabaugh (2010); see also the "partial equilibrium" approach of Postma & Jakobsen (1996) and Jakobsen and Postma (1999)). Our study seeks to address how redox environment (*i.e.*, the dominant electron accepting process) jointly affects microbial carbon utilization through limitations on thermodynamic yields and depolymerization in structured soils.

While soils have macropores that promote advective/convective movement of water and substrates, micropores within aggregates develop spatial geochemical and microbial heterogeneity (Wilpiszeski et al. 2019). These spaces experience different rates of supply and removal of substrates and metabolic by-products than do macropores, as well as unique development of redox profiles relative to bulk soil (Ying et al. 2013; Hall et al. 2013). For instance, upland soils can develop up to 83% oxygen-limited volume resulting in 27-59% less carbon oxidation than a fully aerobic soil (Sexstone et al. 1985; Keiluweit et al. 2016). Furthermore, reduced soils have been shown to accumulate thermodynamically less favorable, reduced organic carbon (LaRowe and Van Cappellen 2011; Boye et al. 2017; Keiluweit et al. 2017; Hodgkins et al. 2018). Such carbon is expected to inhibit the rate of lower-energy heterotrophic metabolisms including iron oxide mineral reduction and sulfate reduction due to a low thermodynamic yield relative to the cost of ATP production (Jin and Bethke 2003; Stuckey et al. 2016; Keiluweit et al. 2016).

Oxygen depletion co-occurs with the inhibition of oxidative extracellular enzymes utilized notably by white-rot fungi to degrade polyphenolic compounds (Pollegioni et al. 2015). Extracellular oxidative enzymes additionally oxidize reduced metals (e.g. Fe(II), Mn(II)) to

produce oxidative (radical) species and are capable of degrading cellulosic material and hydrocarbons (Sinsabaugh 2010; Cragg et al. 2015). Whereas energetic limitations predict an accumulation of reduced organic species, inactivation of extracellular oxidative enzymes would typically favor accretion of relatively oxidized organics such as lignin. Moreover, the dominant electron accepting process in a soil could interact with metabolite and extracellular enzyme production and activity (Freeman et al. 2001; Sinsabaugh et al. 2005), thus altering soil carbon profiles across redox environments.

To encompass redox-mediated limitations on carbon cycling in the context of structured soils, we utilized a dual-pore domain reactor (Fig. S1; *e.g.* Keiluweit et al. (2017); Jones et al. (2018)) that allows diffusion of media into a soil profile from an advective channel, thus establishing a redox (and energy) gradient. In departure from Keiluweit et al. (2017), we challenged soils with added terminal electron acceptors (TEAs), nitrate and sulfate, to observe how TEA supply along preferential flowpaths can alter carbon mineralization and composition responses to alleviation of energetic limitations on the electron-accepting side of metabolisms. Along our constructed redox gradient, we analyzed organic carbon and redox chemistry to ultimately attribute carbon cycling patterns to energetic or enzymatic limitations. Based on redox potential, nitrate was expected to significantly enhance carbon mineralization and to enhance microbial utilization of organic carbon from a range of oxidation states, while sulfate was expected to minimally impact soil processes due to the large presence of iron (oxy-hydr)oxides in the soil, which we anticipated to serve as a similarly favorable electron acceptor. In addition to energetic limitations, we expected to see non-hydrolysable compounds such as lignin and lipids accumulate in anoxic portions of the reactors in accordance with microbial

extracellular oxidative enzyme (*e.g.*, phenol oxidase, phenol peroxidase) requirements for molecular oxygen, thus constituting an enzymatic limitation on microbial carbon cycling.

Methods

Reactor Setup

Soils were collected from the Woodburn soil series, a fine-silty, mixed, superactive, mesic Aquultic Argixeroll, at the Hyslop Field Station (Oregon). The soil was well-drained silt loam adjacent to agricultural research fields and dominated by grassland vegetation (*Agrostic capillaris*, *A. stolonifera*, and *Hypochaeris radicata*). Samples were taken from the A horizon beneath a plow pan (10 – 30 cm), sieved through 2 mm mesh, and stored air-dried until use. General soil characteristics are described in Table S1.

Reactor soils comprised a 1:1 (mass/mass) ratio of air-dried field soil and acid-washed quartz sand separated into the >150 μm fraction to improve diffusion into the soil column by increasing porosity. The soil:quartz mixture consisted of 63 g soil and 63 g acid-washed quartz sand that were thoroughly mixed in a 50 mL Falcon tube, transferred to a beaker, and then mixed to a slurry with 37 mL groundwater media. The slurries were inserted into reactors via the top sampling port (see Fig. S1) using a 30 mL plastic syringe with the tip cut off to give an opening of about 5 mm. Soil slurries were allowed to settle overnight after which media was added at 0.06 mL/min horizontally above the soil surface using 8-channel peristaltic pumps (Ismatec) and 0.64 mm ID PVC pump tubing (FisherBrand) with gas-tight PEEK tubing connecting to reactor ports (SigmaAldrich, OD 0.159 cm x ID 0.076 cm). Groundwater media composition matched field soil solution chemistry: 23 μM $CaCl_2$, 8 μM KCl, 10 μM NaCl, and 5 μM NaH_2PO_4. Four terminal electron acceptor (TEA) treatments received groundwater media with either 1 M $CaSO_4$

143 (SULF), 5 M $NaNO_3$ (NIT), both $CaSO_4$ and $NaNO_3$ added at 1 M and 5 M, respectively
144 (SULFNIT), or unamended media (CON for control). TEA concentrations were chosen based on
145 values typically utilized for culturing denitrifiers or sulfate reducers to ensure the establishment
146 of a gradient in microbial metabolic potential with depth and across treatments. All media were
147 autoclaved, cooled and then connected to peristaltic pump tubing and tubing to house gas lines
148 using sterile technique. All TEA treatments received 0.22 µm-filtered bubbled house air
149 throughout the experiment to promote oxygen saturation and mimic upland soil conditions.
150 NIT, SULF and CON treatments were in triplicate while SULFNIT was in duplicate.
151 Effluent was passed through PEEK tubing through a 0.22 µm PES filter (Sartorius) and collected
152 into 250 mL autoclaved serum vials previously purged with 0.22 µm-filtered nitrogen. Gas bags
153 (Chemware, FEP with septum fitting) were connected to these collection vials via PTFE tubing,
154 a PEEK one-way valve, and 18G x 1 ½ G needles (BD) to collect gases evolved from the
155 effluent under atmospheric pressure. Every two days, reactor effluent was cut off using a PEEK
156 one-way valve, the pumps were turned off, and effluent as well as headspace gas from the gas
157 bags were collected for analysis. The experiment was carried out for 40 d at room temperature
158 and covered from light.
159 Reactors contained ports on the top through which dissolved oxygen was measured with
160 a Unisense 100 µm DO microprobe and Unisense Motorized MicroProfiling System to
161 determine oxic layer depth. Unisense 50 µm pH and H_2S probes were also used to establish the
162 presence of redox gradients. Three microrhizon porewater samplers (Rhizosphere Research
163 Products) with 0.15 µm porous membrane, 8 mm in length, were stationed at approximately 0.5,
164 2, and 5 cm from the top of the soil profile (Fig. S1). These ports and the effluent, which we call
165 a 0 cm depth sample for the sake of comparison, were sampled 10 d into the experiment (to test

166 extraction efficiency; too little water collected for analysis) and at the end of the experiment by
167 drawing a vacuum via a 10 mL syringe (BD) for 2 h with pumps and effluent off, then
168 distributing samples into a) 1 M anoxic HCl for metal analysis via the Ferrozine method
169 (Stookey 1970) and inductively coupled plasma optical emission spectrometry (ICP-OES; ICAP
170 6300 Duo View fitted with a solid state CID Detector), or b) autoclaved microcentrifuge tubes
171 stored in the dark at -20 ^{o}C for future analysis by carbon K-edge near-edge X-ray absorption fine
172 structure (NEXAFS; see below) spectroscopy , Fourier-transform inductively coupled resonance
173 mass spectrometry (FT-ICR-MS; see below), and ion chromatography (Dionex DX-500 fitted
174 with IonPac AS10 column and an electrochemical detector).
175
176 ***Aqueous Chemistry***
177 Ten mL of effluent was collected every-other day in 15 mL falcon tubes, immediately
178 measured for pH, and then frozen until total organic carbon (TOC) measurements the next day.
179 Aqueous concentrations of dissolved organic carbon (DOC) and dissolved inorganic carbon
180 (DIC) were quantified using a Shimadzu TOC-L Total Organic Carbon Analyzer. Due to
181 equilibration of DIC species with vial headspace, 12 mL gas bag samples were taken using
182 airtight 15 mL nylon syringes and stored overnight until measurement by gas chromatography
183 (GC; Shimadzu GC-2014 equipped with an FID and ECD detector) instrument the next day.
184 Gaseous carbon dioxide, nitrous oxide, and methane were measured and concentrations
185 extrapolated back to effluent concentrations using Henry's law. This extrapolation method was
186 used for DIC data to overcome potential loss of DIC in storage prior to TOC analysis.
187 Porewater samples were taken over ice to the Canadian Light Source spherical grating
188 monochromator (SGM) 11ID-1 beamline for carbon K-edge NEXAFS spectroscopic analysis

189 (Regier et al. 2007). Approximately 100 µL of a sample was drop-deposited onto gold-coated
190 silicon wafers in sequential 20 µL drops left to dry under vacuum. A citric acid standard was
191 also prepared in this manner for downstream energy calibration. A single Amptek silicon drift
192 detector (SDD) at 90° horizontal position with respect to the incident beam, to eliminate
193 scattered photons, was used to record the C K-edge NEXAFS spectra. Samples were slew
194 scanned with a beam spot size of 50 x 50 μm^2 at about 20 Hz and for 60 s, collecting between 30
195 to 75 spectra from 275 to 300 eV, each from a new spot on the sample to avoid beam damage
196 artifacts (Gillespie et al. 2015). The spectra were interpolated at 0.1 eV and averaged using a
197 python script written by the SGM beamline staff as a custom NexPy plugin. Spectra were
198 normalized to beam intensity (I_0) by measuring the scatter intensity from an Au-coated Si wafer,
199 averaging over 150 spectra, each spectrum collected from a new spot. Gold scans conducted
200 before and after all samples confirmed no drift in incident beam flux throughout the experiment.
201 Gaussian peak fitting of the averaged normalized spectrum was conducted using Athena (see
202 Electronic Supplementary Material, Table S2). Areas of observed peaks, not including two anti-
203 bonding peaks that were fitted, were used to calculate the relative abundance of seven organic
204 functional groups for downstream processing (quinonic, aromatic, phenolic, aliphatic,
205 amide/carboxylic, alcohol (R-OH), and carbonyl/carbonate C; Keiluweit et al. (2017)).
206 A 12-T FT-ICR-MS spectrometer located at the Pacific Northwest National Laboratory's
207 Environmental and Molecular Science Lab in Richland, WA was used to collect high-resolution
208 mass spectra of the organic matter in the aqueous extract by direct injection in negative ion
209 mode. Samples were first concentrated and desalted using solid phase extraction (SPE)
210 according to Dittmar et al. (2008). Samples were eluted in methanol using 1mL SPE cartridges
211 and introduced directly to the electrospray ionization (ESI) source. The instrument settings were

optimized by tuning on a Suwannee River fulvic acid (SRFA) standard purchased from the International Humic Substances Society (IHCC). Blanks (HPLC grade methanol) were analyzed at the beginning and end of the day to monitor potential carry-over from one sample to another. The instrument was flushed between samples using a mixture of water and methanol. The ion accumulation time (IAT) was varied to account for differences in C concentration between samples. One hundred and forty-four individual scans were averaged for each sample and internally calibrated using an organic matter homologous series separated by 14 Da (CH_2 groups). The mass measurement accuracy was <1 ppm for singly charged ions across a broad m/z range (100–1,200 m/z). Data analysis software (BrukerDaltonik version 4.2) was used to convert raw spectra to a list of m/z values by applying the FT-ICR-MS peak picker module with a signal-to-noise ratio (S/N) threshold set to 7 and absolute intensity threshold to the default value of 100. Putative chemical formulae were assigned using Formularity software (Tolić et al. 2017) based on the following criteria: S/N > 7 and mass measurement error < 1 ppm, taking into consideration the presence of C, H, O, N, S, and P and excluding other elements. In R, assigned peaks were separated from unassigned peaks to facilitate downstream analysis based on elemental composition of samples. Nominal oxidation state of carbon (NOSC; see Electronic Supplementary Material Equation 1), hydrogen to carbon ratio (HC), oxygen to carbon ratio (OC), and double bond equivalent (DBE) were calculated for each assigned peak. Peaks were also separated into eight compound categories –lipids, unsaturated hydrocarbons, condensed aromatic hydrocarbons, proteins, aminosugars, carbohydrates, lignins and tannins –on the basis of their HC and OC values (Boye et al. 2017). Counts and relative abundance of unique peaks observed for each van Krevelen-assigned compound class were calculated for downstream data analysis.

Reactor porewater redox chemistry, DOC concentrations and NOSC were used to model the favorability of dominant microbial metabolisms in six TEA/depth combinations (see Electronic Supporting Material) to assess the extent of organic electron-donor limitations on respiration in the reactors. The model explores how the relationship between NOSC and overall thermodynamic favorability of heterotrophic metabolism depends on electron acceptor identity.

Solid Phase Chemistry

After total carbon production rates stabilized between 28 and 38 d, redox-indicative profiles (O_2, H_2S, and pH) were taken and reactors were disassembled for solid sampling. Soils were partitioned into six depths. The first depth, D1, corresponds to the portion of the soil containing dissolved oxygen above the detection limit in pore water and averaged around 0.4 cm (Fig. S2). Given the heterogeneity of the soil profile, we considered DO values above the detection limit to constitute the "oxic layer", D1. Each subsequent depth collected (D2 – D5) was 1 cm thick except for the final depth, D6, which was between 1 and 2 cm thick. Porewater samplers generally corresponded to depths 1, 3, and 5 (Fig. S1); slight differences across reactors depended on how the soils settled and how the microrhizon samplers flexed with soil addition. For analysis, we consider porewater to be taken from 0, 0.5, 2 and 5 cm and solid samples from 0 – 0.5 cm (D1), one cm increments for D2 through D5, and the remainder corresponding to D6.

For each depth interval, triplicate samples of 1 g were taken to calculate wet/dry weight, another set of 1 g samples was taken for anaerobic incubations, duplicate 0.25 - 0.5 g samples were taken for metal extracts, and leftover soil was frozen at -80 ^{o}C for microbial (not included here) and spectroscopic characterization. Water content was determined by drying soil samples at 50 °C; soils were considered dry when the weight change was less than 1% overnight, which

took 1 week. Anaerobic incubations measuring "respiration potential" were performed in 10 mL amber serum vials that were stoppered in the glove bag after adding 2 mL anoxic, sterile milli-Q water and shaken vigorously to mix soil. Vials were sampled in duplicate after 30 h, still within the range of linear CO_2 production rates, via gastight syringe and analyzed by GC. Anoxic 0.5 M HCl was added to metal extract samples in 25 mL acid-washed serum vials that were then thoroughly hand shaken and placed on an orbital shaker (VWR, 145 rpm) for 1 h at room temperature. Suspensions (1.5 mL) were centrifuged at 12,500 rcf anaerobically and 0.5 mL were then pipetted into 9.5 mL of 2% anoxic nitric acid for ICP-OES measurement and into 0.5 mL 1 M anoxic HCl (water boiled, HCl added, and nitrogen-sparged for 2 h until cool) for analysis by the Ferrozine assay (Stookey 1970) modified for 96-well plates. Briefly, 10 µL of each acidified sample was added in duplicate to one plate containing 90 µL of 1 M HCl (Fe(II) determination) and to a second plate containing 90 µL of 50% w/w hydroxylamine HCl in ammonium acetate (total Fe determination). Both plates then received an additional 100 µL of ferrozine reagent and were mixed with pipetting, allowed to incubate for 20 min, and followed by absorbance measurements at 562 nm on a Synergy HTX Multi-Mode Reader (BioTek).

Statistical Analysis

All statistical analysis and data visualization not described above was performed in RStudio version 1.1.383 (RStudio Team 2016). For bulk measurements such as cumulative DIC production, one-way ANOVA was used to assess significance between different TEA treatments. For measurements taken from different depths and for different TEA treatments, two-way ANOVA was performed. Tukey's Honestly Significant Difference test was used for post-hoc analysis.

Solid and aqueous phase data were compiled and the composite dataset containing all measured variables was used for correlations and hierarchical tree building. A dataset lacking FT-ICR-MS variables was additionally used in principal component analysis (PCA) to restrict the larger number of factors versus observations (31 vs. 33 in the full dataset and 31 vs. 41 in the dataset with FT-ICR-MS variables removed). Correlations and clustering were also performed on the dataset without FT-ICR-MS (Fig. S9).

Spearman rank correlations were performed using the R rcorr function. No data transformations were performed as all correlations appeared linear for pairs exhibiting trends. The correlation matrix output was transformed to remove negative values by subtracting the correlation coefficient from 1 and then converted into a distance matrix. This distance matrix was used to perform hierarchical clustering with the function hclust, choosing "complete" linkage to provide a less biased tree. The corrplot package was used to visualize correlation coefficients, p-values and clustering of variables based on a built-in hclust function.

PCA was performed using the function prcomp. Depth was included as a factor, whereas TEA treatment was only added as a visual effect to identify trends among factors. PC loadings were taken directly from the PCA output. In general, this approach was used to interpret the combined influence of TEAs and depth in the context of a soil profile on overall soil redox and carbon chemistry.

Results

Bulk Carbon Production

Total inorganic (TIC) and dissolved organic carbon (DOC) production increased throughout the 40-day experiment for all TEA treatments, and the cumulative amounts varied

between treatments ($p=0.0097$; Fig. 1a). At around 10 d, TIC production slightly decreased, continuing to increase thereafter and approaching a constant production rate after about 28 d. This pattern was mirrored in the DOC data. TIC production was greatest in the NIT and SULFNIT treatments compared to SULF and CON ($p\approx0.045$ for SULFNIT vs. CON and NIT vs. SULF; $p=0.013$ for NIT vs. CON; SULFNIT vs. SULF not significantly different). TEA treatment led to differences in cumulative DOC production in reactor effluent ($p<0.001$; Fig. 1b). DOC production was greatest in NIT and SULFNIT, which were both higher than SULF ($p=0.002$ and $p=0.021$) and CON ($p=0.002$ and $p=0.018$, respectively).

Redox Profiles

Redox-active elements – particularly the spiked TEAs – developed depth-gradients indicative of increasingly reducing conditions with depth (Fig. 2). Nitrate in the NIT and SULFNIT media (1650 μM occurs at 0 cm depth) was increasingly consumed between 0, 0.5 and 2 cm and completely consumed within 5 cm of the advective channel, while in SULF and CON treatments it did not vary with depth (Fig. 2a). Nitrite concentrations at the surface were 0 – 4.6 μM and generally increased with depth to between 17.3 – 37.4 μM except for SULFNIT, for which nitrite peaked at 0.5 cm, and the control, which had slightly lower nitrite at 0.5 cm than at the surface (Fig. 2b). In contrast to nitrate, SO_4^{2-} was minimally depleted by about 100 μM between 0.5 and 5 cm in the SULF treatment, with only a small SO_4^{2-} decrease at 0.5 cm in SULFNIT (Fig. 2c). Sulfate concentrations in NIT treatments increased with depth (Fig. 2c). Porewater Fe(II) concentrations ranged from 0.012 mM at the surface to 0.153 mM at 5 cm (Fig. 2d). The SULF treatment produced significantly more Fe(II) at intermediate depths than other TEA treatments (Fig. 2d).

Fe and Mn concentrations in acid extracts, inferred to be predominantly Fe(II) and Mn(II), generally increased with depth and paralleled each other with respect to depth trends vs. treatment, with the most modest increase always in the NIT and SULFNIT treatments (Fig. 3). Manganese concentrations ranged from 1.5 – 7.4 μmol $(g\ soil)^{-1}$ with the highest values observed in SULF and SULFNIT treatments (Fig. 3a). Fe concentrations ranged from 17.9 – 101.2 μmol $(g\ soil)^{-1}$, with CON, SULF and SULFNIT all higher than the NIT treatment (Fig. 3b). In a departure from other treatments, SULFNIT acid extract concentrations of Mn and Fe peaked in the middle of the soil column (3.5 cm; Fig. 3), although CON reactors also peaked in acid-extractable metals at 4.5 cm (Fig. 3). In general, the addition of nitrate suppressed dissolved and acid-extractable Fe and Mn production throughout the soil profile, whereas the addition of sulfate appeared to generate more or similar amounts of dissolved Fe and Mn as the CON treatment (Fig. 3).

Carbon Concentrations and Respiration

Porewater DOC concentrations significantly differed across depths ($p<0.001$) and treatments ($p=0.016$) (Fig. 4a). DOC was overall higher at depth, with concentrations at 5 cm greater than at 2.5, 0.5 and 0 cm ($p<0.001$ for all) and with 2.5 cm having higher DOC than at 0 and 0.5 cm ($p<0.01$ each). For CON, SULFNIT and NIT treatments, DOC was significantly higher at 5 cm than at 0 cm ($p<0.012$). In terms of treatment, CON had significantly higher DOC than SULF reactors ($p=0.026$) and marginally significantly higher DOC than SULFNIT and NIT reactors ($p = 0.061$ and 0.097, respectively). DOC was highest in the CON treatment over the first 2 cm and matched by SULF, NIT and SULFNIT at 5 cm. Porewater DIC

concentrations did not show consistent trends with depth ($p=0.53$) or between TEA treatments ($p=0.43$; Fig. 4b).

Anaerobic incubations of soils collected across the depth gradient for each treatment showed significant differences with depth in CO_2 production ($p=0.038$), particularly being higher at 6 cm than at 0.5 cm ($p=0.041$) (Fig. 4c). The highest CO_2 production at 0 cm was from SULFNIT (3.44 mg C $(g\ soil)^{-1}$) followed by NIT (2.53 mg C $(g\ soil)^{-1}$). In the bottom 3 cm of the soil profile, the highest CO_2 production was from CON (roughly 4.6 mg C $(g\ soil)^{-1}$). Treatment also explained differences in CO_2 production ($p=0.037$), with SULF being significantly lower than CON ($p=0.042$). Methane production was negligible for all reactors but NIT, where CH_4 production declined from 0.025 mg CH_4-C $(g\ soil)^{-1}$ at 0.5 cm to 0.020 mg CH_4-C $(g\ soil)^{-1}$ at 6 cm but peaked at 4.5 cm at 0.057 mg CH_4-C $(g\ soil)^{-1}$ (Fig. S3a). Nitrous oxide production was between 1.5 and 7.6 μg N_2O-N $(g\ soil)^{-1}$ at 0.5 cm and declined with depth (not statistically significant) for all treatments except for SULF, which remained constant with depth (Fig. S3b). N_2O production in NIT spuriously increased to .0091 mg N_2O-N $(g\ soil)^{-1}$ at 6 cm.

Porewater Organic Carbon Chemical Composition

Water-extractable organic carbon was analyzed by FT-ICR-MS and from the C K-edge NEXAFS spectra to determine the relative abundance of functional groups and compound classes and to understand the thermodynamic favorability of the microbially accessible DOC pool. In general, NOSC declined with increasing depth in the reactors (Fig. 4d). Average NOSC declined significantly with each depth increment in NIT ($p<<0.001$). The 0 cm and 2 cm NOSC values in SULFNIT did not differ from 0.5 cm ($p=0.09$ and 0.17), but for all other comparisons,

NOSC was lower at greater depths ($p<0.001$). SULF NOSC was significantly lower at greater depths ($p<0.003$) except for the 0.5-2 cm and 2 cm-5 cm pairs ($p=0.14$ and 0.10). The notable exception was the control treatment, which maintained a constant NOSC with depth ($p>0.14$ for all depth comparisons; Fig. 4d).

Gibbs free energy of reaction and thermodynamic factor, F_T (Jin and Bethke 2005), were calculated for dominant redox couples as a function of NOSC (Fig. 5; further details in Electronic Supplementary Material). Across the range of NOSC values, F_T for denitrification and oxic respiration at the soil-macropore interface (*i.e.* the soil surface in the reactors) was essentially 1, meaning carbon oxidation rate was thermodynamically uninhibited. Denitrification at 5 cm, which has lower NO_3^- concentrations than 0 – 0.5 cm, became slightly less favorable than at the surface ($F_T < 1$ and less negative ΔG_{rxn} at lower NOSC values; Fig. 5). Sulfate reduction at both 0-0.5 cm and 5 cm depth depended heavily on NOSC, with F_T dropping to 0 between NOSC values of 1 and 2. Ferrihydrite reduction, which was modeled for CON reactors at 5 cm, was even less favorable than sulfate reduction at NOSC values below about 3 (Fig. 5b). The ΔG_{rxn} for metabolisms utilizing low-energy TEAs (SO_4^{2-}, ferrihydrite) depended heavily on NOSC, ranging over 800 kJ $(mol\ C)^{-1}$ across the NOSC range (Fig. 5b).

Across all TEA treatments, the most abundant compound classes by FT-ICR-MS were lignin, lipids, condensed aromatics, and proteins (Figs. S4, S5). Lipid relative abundance declined going from 0.5 cm to 5 cm depth, although this pattern is less clear for the NIT and SULFNIT treatments (Fig. S5). Tannins and unsaturated and condensed aromatic hydrocarbons appeared to decline in relative abundance with depth for added TEA treatments but to increase or remain constant with depth in the control (Fig. S5). Lignin relative abundance increased with increasing depth across all treatments, although the trends in NIT and SULFNIT are less clear

(Fig. S5). Relative abundance of hydrolysable proteins, carbohydrates and aminosugars did not change with depth (Fig. S5). The average NOSC of various compound classes did not differ across TEA treatments; however, the average NOSC of tannins and condensed hydrocarbons decreased with depth for all but CON and NIT reactors, respectively (Fig. S6).

The high relative abundance of aliphatics that decreased with depth observed in NEXAFS data (Fig. S7) agreed with lipid patterns from FT-ICR-MS data. Other NEXAFS-derived moieties that decreased in relative abundance with depth were aromatics (all treatments) and quinones (NIT treatment; Fig. S7), which corresponds to a decline in condensed aromatics and tannins with depth (Fig. S5). In contrast, the amide/carboxyl moiety (corresponding to FT-ICR-MS protein and lignin counts) appeared to increase with depth in all but the NIT treatment (Fig. S7). Phenolics followed a similar pattern of increasing with depth most notably for the low-energy CON and SULF reactors (Fig. S7). The trends between functional groups (C-NEXAFS data looking at all DOC < 0.22 μm) and corresponding polymeric compounds in which they would be present (FT-ICR-MS data capturing 100 to 1,200 g molecular weights) suggest that low-molecular weight compounds microorganisms might use in respiration generally reflect the composition of their polymeric precursors.

Correlations and Visual Analysis

Correlations between factors were visualized to determine how soil structure-induced redox gradients altered carbon chemical profiles with depth. Spearman correlations revealed that common indicators of reducing conditions such as acid-extractable Mn and Fe concentration were highly correlated to one another and to concentrations of organic compounds traditionally

known to accumulate at depth under more anoxic conditions, including phenolics and lignin (Fig. 6, Cluster 5). This cluster also included porewater Fe and both Fe(II) and total acid-extractable Fe, double bond equivalents, amide/carboxyl structures, alcohol structures, dissolved inorganic carbon, and sulfate. Another cluster of factors (Fig. 6, Cluster 4) was dominated by compounds showing strong negative relationships with depth: NOSC, OC, anaerobic N_2O production potential, and the relative abundance of condensed aromatic hydrocarbons and quinone and aromatic functional groups. DOC/TC (which were essentially equivalent) clustered most closely with depth of all factors and were closely related to nitrite concentrations, the ratio of acid-extractable Fe(II)/Fe(total), pH, and the relative abundance of protein and carbonyl-C (Fig. 6, Cluster 3). A fourth grouping showed strong anti-correlations with depth and comprised lipids, carbohydrates, HC, dissolved oxygen, amino sugars, aliphatic carbon, unsaturated hydrocarbons and tannins (Fig. 6, Cluster 2). Finally, nitrate grouped most closely with methane and carbon dioxide production potential (Fig. 6, Cluster 1).

Principal component analysis was used to attribute differences in sample chemistry to either distance from the macropore (*i.e.* depth) or dominant electron accepting process (*i.e.* TEA treatment). Principal component analysis revealed a clear separation of depth classes driven strongly by PC1 (29.2% of variance explained; Fig. 7a). While PC1 appears to separate samples according to depth, other factors have similarly high absolute value loadings on PC1 to depth (Fig. S13). These factors include phenolic and amide/carboxyl relative abundance, DOC concentration, porewater Fe, pH, and (negatively correlated) aliphatic relative abundance and NO_3^- and O_2 concentration (Figs. 7a, S13). Intriguingly, aliphatic relative abundance was almost completely anticorrelated with depth in the PC1 vs. PC2 projection (Fig. 7a). Grouping samples by treatment revealed that PC2 (14.8% variance explained) somewhat separates TEA treatments

(Fig. 7b), particularly SULF and NIT, based on CH_4 production, acid extractable metal concentrations, and the relative abundance of aromatics, quinones, and alcohols. PC4 also appears to separate on the basis of treatment: in a biplot with PC2, it separates CON and SULF from SULFNIT predominantly based on amide and aromatic relative abundance, N_2O production potential, and Fe(II)/Fe(total) (Fig. S11). Only PC1 appears to separate samples based on depth (Fig. S10).

Discussion

Through the establishment of a redox gradient in a formerly uniform upland topsoil, we examined the influence of various exogenous electron acceptors on carbon utilization and microbial respiration. Our dual-pore domain reactor setup removed the environmental possibilities of carbon deposition or horizonation, preexisting functional differences in microbial communities, varying soil textures and structures, and distinct carbon chemistry and age, thus promoting a focus on electron acceptor availability. Redox stratification and TEA availability were therefore the main variables controlling differences in microbial carbon processing with depth. We expected the reducing conditions developed at depth would drive NOSC to low values that do not support microbial carbon oxidation (Boye et al. 2017; Keiluweit et al. 2017; Bhattacharyya et al. 2018), constituting an "energetic limitation" on microbial carbon processing. The lack of oxygen beyond roughly 0.5 cm would additionally constitute an "enzymatic limitation" that inactivates extracellular oxidative enzymes (Sinsabaugh 2010), leading to an accumulation of common oxidative enzyme substrates such as lignin and char (Freeman et al. 2004).

461

462 ***Redox Zonation***

463 By 40 days, all reactors had developed a distinct redox gradient: oxygen was depleted
464 near the surface (Fig. S2a) followed by nitrate or sulfate depletion in SULF, NIT and SULFNIT
465 treatments and then accumulation of reduced Mn and Fe deeper than 3 cm (Figs. 2, 3). NIT and
466 SULFNIT reactors respired the most CO_2 (Fig. 1), consistent with nitrate providing a more
467 favorable thermodynamic driving force compared to other anaerobic respiration pathways
468 (McLatchey and Reddy 1998). However, we discuss below the potential for N addition
469 alleviating N limitations. Respiration in SULF reactors only marginally (and insignificantly)
470 exceeded that of CON reactors (Fig. 1). Sulfate reduction appears limited in this experiment
471 relative to its supply rate as SO_4^{2-} concentrations varied only to a maximum of 22% from initial
472 media concentration (Fig. 2c). Nitrate, by contrast, was almost completely consumed at 5 cm
473 (Fig. 2a). The loss in NO_3^- appears to be driven by denitrification given the peak in N_2O
474 emissions near 0 cm and the corresponding absence of NO_2^-, presumably due to rapid
475 consumption by denitrifiers or chemodenitrification (Figs. 2, S3b; Tiedje (1988); Grabb et al.
476 (2017)). No hydrogen sulfide was detected throughout the soil profiles; sulfide was likely
477 consumed by reaction with other soil constituents (*e.g.*, Fe(III) minerals, as suggested by the high
478 porewater Fe and acid-extractable Mn and Fe in SULF reactors (Figs. 2d, 3) (Koretsky et al.
479 2003; Poulton 2003; Canfield et al. 2010; Hansel et al. 2015). Overall, sulfate addition had a
480 limited impact on bulk respiration or DOC production compared to control reactors, suggesting
481 adequate sulfur for microbial respiration and minimal enhancement in respiration energetics.
482 Regardless of non-respiratory chemical reactions, redox gradients were clearly established as a
483 function of depth, and unique metabolic regimes were achieved between TEA treatments.

Patterns in Microbial Respiration

Energy of Redox Couples

Reactors with added TEAs all showed higher cumulative total inorganic carbon production, a proxy for respiration (Fig. 1a). This and the higher DOC concentrations observed in NIT and SULFNIT reactor effluents (Fig. 1b) suggest enhanced microbial utilization of soil carbon given abundant and favorable electron acceptors. Nitrogen limitation and subsequent fertilization would also explain some increased DOC production and respiration with added nitrate. The field soil C:N value of 15.0, however, suggests that N is not severely limiting (Brady and Weil 2008). SULF reactors had lower anaerobic respiration potential than NIT reactors in the top 2 cm (Fig. 4c), suggesting that lower thermodynamic potential of sulfate reduction compared to denitrification (or N-limitation) limits respiration at the macropore-soil interface rather than electron donor limitations because NOSC and DOC concentration for SULF and NIT were equivalent in the top 1 cm.

The rapid decline in NIT NOSC and shallower decline of SULF and SULFNIT NOSC with depth (Fig. 4c) highlight microorganisms' preferential use of oxidized organic carbon given abundant electron accepting capacity. Somewhat lower porewater DOC concentrations in all added-TEA treatments compared to CON at intermediate depths (Fig. 4a), and lower anaerobic respiration potential in added-TEA treatments compared to CON (Fig. 4c), further support that higher electron accepting potential in soils contributes to a rapid consumption of microbially available carbon. Specifically, thermodynamically favorable high-NOSC carbon is rapidly consumed given ample energy from available TEAs, resulting in energetically preserved DOC

506 that does not support anaerobic respiration (Fig. 4). While these trends were only statistically
507 significant in the SULF-CON comparison, the higher bulk DOC production in NIT treatments
508 along with higher respiration (Fig. 1), but somewhat lower porewater DIC, strongly suggest that
509 some combination of nutrient addition, favorable energetics and microbial community
510 composition or activity favored DOC production in NIT reactors (Fig. 4). Such an interpretation
511 would suggest gross DOC consumption in NIT reactors exceeded that in CON despite the lack of
512 significant differences in observed porewater DOC concentrations, and the consumed carbon was
513 on average more oxidized and energetically favorable, leading to low NOSC in the NIT
514 treatment.

515

516 *Organic Electron Donor Concentration*

517 Figure 4 additionally highlights a dual electron-donor limitation driven by both low
518 concentrations of microbially available organic carbon and low carbon favorability (*i.e.*, low
519 NOSC). Since only CON had higher respiration than other treatments past 3 cm despite having a
520 lower NOSC (with the exception of NIT; Fig. 4c,d), the concentration of DOC rather than its
521 oxidation state appears to drive anaerobic respiration potential (Stegen et al. 2018). The higher
522 CO_2 production of NIT and SULFNIT reactors at 0 cm (Fig. 4c) can be explained by nitrate
523 competing with oxygen as a favorable electron acceptor, thus resulting in greater O_2 abundance
524 and thus respiratory potential on the electron acceptor side. Residual nitrate at these shallow
525 depths (Fig. 2a) and higher oxidative enzyme activity would also explain higher anaerobic
526 respiration potential at the surface of added-NO_3^- reactors. The observation that both DOC
527 concentration and CO_2 production are driven down in SULF compared to CON despite similar
528 energetic favorability of iron oxy-(hydr)oxide and sulfate reduction (Fig. 5) suggests that we

529 have selected for an energetically limited and thus slow-respiring community in SULF reactors.
530 Selection of fermenters seems likely given how alcohols (alkyl-OH) align with sulfate in PC2 of
531 Fig. 7b, which separates NIT from SULF reactors.

532

533 ***Energetic Limitations on Microbial Respiration***

534 Higher dissolved organic carbon concentrations with lower average NOSC at depth
535 indicate a potential mechanism of preservation of SOC in structured soils through energetic
536 limitations. Regardless of TEA treatment, reactors had higher DOC concentrations at 2.5 and 5
537 cm than at 0 cm (Figs. 4a, 6). Furthermore, DOC clearly separates samples by depth along PC1
538 (Fig. 7a). Following the energetic limitations hypothesis, a lack of energy from the organic
539 electron donor/ambient (or added) electron acceptor couples would result in slower DOC
540 processing and its resulting accumulation at depth. Indeed, the onset of reducing conditions (*i.e.,*
541 higher acid-extractable Fe(II), a higher Fe(II)/Fe(total) ratio, and higher porewater Fe) positively
542 correlates with DOC concentrations (Fig. 6a). The negative correlation of DOC with dissolved
543 oxygen, NOSC and OC further connects reducing conditions with DOC accumulation. Because
544 highly oxidized (high NOSC) carbon is more favorable as an electron donor, high-NOSC carbon
545 is preferentially consumed in reducing environments that provide less metabolic energy through
546 the electron acceptor (LaRowe and Van Cappellen 2011). This process leaves behind more
547 reduced organic carbon under anaerobic conditions (Boye et al. 2017; Keiluweit et al. 2017;
548 Bhattacharyya et al. 2018). Such a process likely contributed to the accumulation of lower
549 average-NOSC and higher HC ratio carbon deeper in the reactors, and importantly would lead to
550 its continued preservation due to poor thermodynamic favorability. It is worth noting, however,
551 that iron dissolution also releases formerly mineral-protected carbon to the dissolved phase and

552 could partially explain our correlation between reduced iron and DOC with depth (Hall et al.
553 2015). However, this seems unlikely in these soils given that NIT reactors did not experience
554 increased acid-extractable or porewater Fe despite higher DOC concentrations at depth (Figs. 3,
555 4).

556 Keiluweit et al. (2016) modeled that SO_4^{2-} and Fe(III) supported carbon oxidation only on
557 a subset of compound classes with higher NOSC values. We therefore expected NOSC to be
558 driven to lower values in the CON and SULF reactors compared to NIT and SULFNIT reactors.
559 At the 0 cm, NOSC was practically equivalent between NIT and SULFNIT treatments and
560 insignificantly lower for SULF (Fig. 5). Average NOSC in CON reactors was significantly
561 lower (about -0.40 ± 0.10 (s.d.) vs. -0.230 ± 0.009). Higher NOSC at the surface of added-TEA
562 reactors could be due to generally favorable energetics due to high TEA concentrations relative
563 to CON leading to a) production of energetically favorable oxidized microbial metabolic
564 products and/or b) enhanced energy to consume less favorable, negative-NOSC SOC. In the
565 latter case, as favorable electron acceptors are utilized, only the most oxidized organic
566 compounds should support respiration and thus be preferentially consumed at depth—*i.e.*, under
567 more reducing conditions (Keiluweit et al. 2017; Pracht et al. 2018). The CON NOSC remained
568 constant with depth, likely due to a stable redox status consistent with iron reduction throughout
569 the soil profile. SULF and SULFNIT achieved average NOSC values similar to CON deeper in
570 our reactors, which is consistent with a move from favorable sulfate reduction (at least in these
571 soils; see Fig. 5) and denitrification to iron oxy-(hydr)oxide reduction.

572 To assess the interaction between NOSC and respiration potential, we calculated
573 $\Delta G_{reaction}$ of the oxidation of organic carbon by O_2, NO_3^-, Ferrihydrite, or SO_4^{2-} for each depth ×
574 TEA treatment combination and used this value to assess the thermodynamic limitation of

carbon oxidation using a respiration kinetic model that incorporates microbial electron transport physiology (Jin & Bethke (2005); see Electronic Supplementary Material). Under experimental conditions measured at the end of the 40-day incubation, an F_T of 1 at 0-0.5 cm for oxic respiration and at all depths for nitrate reduction to nitrite was calculated (Fig. 5a). For sulfate and ferrihydrite reduction, however, F_T dropped to zero for all depth x TEA combinations under experimental conditions. Such F_T values indicate a thermodynamic driving force too low to support dissimilatory sulfate and iron reduction—a finding that generally agrees with the sulfate and iron depth trends in Fig. 2. These calculations are generalizations for two reasons: first, they are based on a sample's average NOSC rather than the range; and second, our NOSC calculations are limited to compounds with molecular weights of 100 g or greater –compounds that would require enzymatic breakdown prior to respiration (CITE). Given that FT-ICR-MS and C-NEXAFS compound and functional group profiles align, we suspect the microbially available low-molecular weight carbon parallels the larger compounds observed with FT-ICR-MS. To address the first shortcoming, we modeled F_T for each reaction across a full range of NOSC values and found that only NOSCs more positive than +1.6 (0.5 cm) or +1.4 (5 cm) would support sulfate reduction and NOSCs more positive than +2.2 (5 cm) would support dissimilatory ferrihydrite reduction under the geochemical conditions observed in the reactors (see Electronic Supplementary Material; Fig. 5). While the average DOC compound would not support these less favorable metabolisms, a smaller pool of positive-NOSC DOC must support dissimilatory sulfate and iron reduction in our reactors based on sulfate and porewater iron trends (Fig. 2). This pool is likely recycled by processes such as fermentation or hydrolysis of organic polymers (particulate or mineral-associated) (Coleman 1994). These models highlight the joint dependence of respiration on both the favorability of the electron donor and acceptor. It is also

598 worth noting that our experimental conditions drastically shifted the NOSC-dependence of
599 favorability of various pathways compared to predictions made at standard state (*i.e.* Keiluweit et
600 al. (2016)): we found respiration of ferrihydrite and sulfate to be unfavorable across a greater
601 range of NOSC values and SO_4^{2-} respiration to have a slightly higher F_T for a given NOSC value
602 than ferrihydrite reduction (Fig. 5).

603 Intriguingly, average NOSC in the NIT treatment declined with depth beyond that of CON
604 (Fig. 4d; note that we had too little of the lowest porewater sample to perform this measurement
605 on the 5.0 cm depth). Such behavior of NOSC in NIT treatments appears to counter our original
606 hypothesis that generally favorable energetics promote nondiscriminatory microbial oxidation of
607 organic compounds, meaning negative and positive NOSC compounds would be used at similar
608 rates and NOSC would not be driven to low values (Boye et al. 2017). An alternative hypothesis
609 is that microorganisms –in this case, denitrifiers –tend to compete for favorable, more oxidized
610 organic substrates rather than specialize on different NOSC ranges. This has been observed in
611 batch incubations, where organic acids and carbohydrates are preferred over alcohols and
612 compounds with higher HC values (Mokhayeri et al. 2006; Warneke et al. 2011). Alternatively,
613 nitrate may provide microorganisms enough energy to produce more extracellular enzymes to
614 break down hydrolysable (and more reduced C on average; Fig. S6) polymeric substrates
615 protected by mineral association or as particulate organic matter, leading to a reduced overall
616 NOSC relative to other TEA treatments. Nitrate fertilization has been shown to increase
617 extracellular enzyme production, activity and respiration on many N-limited soils and litters
618 (Fierer et al. 2003; Bach and Hofmockel 2015). Cellulose and N- and P-acquiring enzyme
619 activities increase with N additions, whereas lignin degrading enzymes and lignin decomposition
620 typically are inhibited or unaffected, particularly in mineral soils (Sinsabaugh et al. 2005; Allison

et al. 2009; Keeler et al. 2009). However, the relative abundance of protein, amino sugar and carbohydrate polymers was similar between NIT and other treatments (Fig. S5). We conclude that a preference for oxidized organic substrates drove NOSC to negative values when favorable electron acceptors, possibly particularly NO_3^- and the microbial community it selected for, were present.

Enzymatic Limitations on Microbial Respiration

In support of the enzymatic limitation hypothesis, polymeric compounds requiring oxidative cleavage prior to microbial utilization increased in relative abundance with depth and depleted oxygen levels. These compounds include phenolic structures, amide/carboxyl groups and lignin (Figs. 6, 7, S5 & S7). In contrast to other organic compounds and functional groups, these lignin-like structures' relative abundance increased in a stepwise manner going from 0 cm to 0.5 cm and deeper (Figs. S5 & S7). Especially given that this jump was more pronounced for CON reactors, which theoretically have less competition for TEAs and thus consume oxygen more rapidly in the top 5 mm; it appears to be driven by anoxia specifically rather than increasingly reduced conditions. The clustering analysis grouped phenolic and lignin factors together in a category including porewater Fe and amide/carboxyl groups (C5, Fig. 6b), which also jumped in concentration between 0 and 0.5 – 2.0 cm (Figs. 6b, 2d, S7). This step-increase in lignin, phenolic and carboxyl carbon highlights the difference in control on these lignin-like organics versus total DOC concentrations and the relative abundance of hydrolysable proteins, carbohydrates, *etc*., which increase fairly regularly with depth (Figs. 4a, S5, S7).

642 Accumulation of polyphenolic compounds under anoxic conditions has been noted
643 conceptually and in multiple field settings (Cocozza et al. 2003; Kleber 2010; Fenner and
644 Freeman 2011; Leifeld et al. 2012). In anoxic systems, extracellular oxidative enzymes
645 produced predominantly by fungi are inactivated, which stalls the decomposition of complex
646 polymers such as lignin or condensed aromatic carbon (Kleber 2010). According to the
647 "enzymatic latch" hypothesis, inactivation of extracellular oxidative enzymes should also result
648 in parallel accumulation of organic substrates requiring oxidative and hydrolytic degradation
649 pathways due to phenolics' inhibition of hydrolases (Freeman et al. 2001; Mann et al. 2014; but
650 see Hall et al. 2014 in opposition). However, the abundance of hydrolysable compounds such as
651 carbohydrates, aminosugars and proteins did not correlate with depth in this experiment (Fig. 6).
652 Perhaps our mineral soil lacked the litter-derived lignin/hemicellulose/carbohydrate complexes
653 on which an enzymatic latch mechanism common in organic matter-rich environments would
654 operate. Alternatively, our upland soils likely had relatively low levels of phenolics compared to
655 former studies in peat such that inhibition was minor (Freeman et al. 2001, 2004). Regardless,
656 anoxic conditions promoted the preservation of phenolic carbon in a pattern unique from the
657 general linear increase in DOC with depth, highlighting the co-occurrence of enzymatic and
658 energetic preservation mechanisms acting on soil carbon under reducing conditions.

659

660 ***Deviations from Expected Energetic and Enzymatic Controls***

661 Despite trends in NOSC and lignin-like compounds agreeing with energetic and enzymatic
662 limitations on carbon cycling, other organic compounds' depth trends appeared to undermine
663 these purported mechanisms at first glance. Most notably, lipids strongly anti-correlated with
664 depth (Figs. 6, 7, S5). Lipids have quite a negative NOSC typically between -1.2 and -1.5 (Fig.

665 S6), which as described above and in the literature should not support respiration by ferric iron
666 or sulfate under these experimental conditions and should lead to their accumulation at depth
667 (Hedges and Keil 1995; Lorenz et al. 2007; Pisani et al. 2014). Their anticorrelation with depth
668 can be attributed to a higher microbial biomass near the soil surface (noted in Qubit
669 measurements on CON DNA extracts; Fig. S14). In the recent study by Huang et al. (2020),
670 lipid abundance did not change between anoxic and aerobic incubations. Other studies have
671 shown increased lipid abundance in more microbially active, surface environments (Sengupta et
672 al. 2019), further supporting the production of lipids in or nearer to oxic surface soils
673 overshadowing signals of lipid stabilization with depth/reducing conditions.

674 Other surprises included unsaturated hydrocarbons and condensed aromatic hydrocarbons,
675 which declined in relative abundance with depth for all treatments except for CON, where they
676 respectively increased or did not change with depth (Fig. S5). Unsaturated hydrocarbons can be
677 broken down following hydroxylation and beta-oxidation and thus can, albeit slowly, degrade
678 anaerobically (Schink 1985). Even saturated hydrocarbons appear to undergo radical-mediated
679 substitution reactions followed by decomposition (So and Young 1999; Rabus et al. 2001).
680 Condensed aromatic hydrocarbons can similarly be degraded via carboxylation reactions often
681 observed in denitrifiers or ring reductions observed in sulfate reducers, fermenters and
682 methanogens (Schink et al. 2000; Meckenstock et al. 2004). These trends suggest that overall
683 low metabolic energy availability, (*e.g.* ferrihydrite reduction, which is less favorable than
684 sulfate or nitrate reduction in our reactors; Fig. 5,) can inhibit decomposition pathways not
685 requiring oxygen (Schink 2002).

686 Among the uncontrolled variables in our experiment (*i.e.* microbial community, which was
687 intended to vary), our experimental approach did not account for differences in mineral

688 protection across reactors and depths. Particularly in upland soils, mineral protection can explain
689 upwards of 40% of variation in SOC across chronosequences and climate gradients and can
690 sustain SOC persistence for up to millennia longer than non-mineral associated organic carbon
691 (Torn et al. 1997; Hemingway et al. 2019). Given that our DOC data comes from porewater and
692 does not account for exchange between mineral-associated and porewater carbon pools, it is
693 entirely possible that we have missed dynamics of certain compounds (*e.g.*, plant-derived
694 compounds, aromatics) that sorb strongly to mineral surfaces (Kalbitz et al. 2005; Coward et al.
695 2019). We have chosen to highlight dynamics of microbially-accessible carbon rather than long-
696 term preservation dynamics (Marschner and Kalbitz 2003; Sokol et al. 2019) as our main goal
697 was to assess the potential for structured soils to develop energetic limitations on respiration,
698 which would most strongly affect free organic matter.

699

700 ***Conclusions***

701 The observation of increased carbon preservation with depth in just over one month of
702 experimentation underscores the rapidity with which microbial limitations on carbon oxidation
703 ensue in soil and is consistent with previous work (Keiluweit et al. 2017). The presence of
704 favorable terminal electron acceptors increased bulk respiration at the expense of dissolved
705 organic carbon and drove this same organic carbon to more reduced values unfavorable for
706 respiration. In turn, more reduced carbon limited respiration by the less favorable electron
707 acceptors, sulfate and iron oxy-(hydr)oxides. Phenol groups and lignin, instead of accruing
708 linearly with depth, increased dramatically within 0.5 cm from the soil surface –a trend not
709 shared by other organic compounds across all TEA treatments—thus highlighting the enzymatic
710 limitation on oxidation of lignin-like carbon. We have shown that a tight interplay between

electron donor and acceptor thermodynamic favorability controls soil respiration, and structured soils develop diverse metabolic regimes with differing potential to oxidize SOC over short timescales. Whereas historically stabile soil carbon has been thought to accrue as a function of centuries to millennia of depletion of "labile" organic matter (Sollins et al. 1996; Lützow et al. 2006), we highlight here a key role for reducing conditions in preserving SOC. Not only do reducing conditions drive remaining SOC to less favorable negative NOSC values on average (resulting in, for example, accumulation of hydrocarbons and alcohols at depth; Baldock et al. (1997); Lichtfouse et al. (1998); Almendros et al. (1999)); they inhibit oxidative enzyme activity that depolymerizes plant polymers for downstream oxidation. In the context of ecosystem factors' contribution to SOC persistence (Schmidt 2012), redox potential clearly drives the quality and composition of SOC and thus its likelihood of consumption by microorganisms.

Declarations

Funding: This work was funded by a National Science Foundation Graduate Research Fellowship to H.R.N. and a Department of Energy Biological and Environmental Research, Subsurface Biogeochemistry Program award (Award Number DE-SC0016544) to S.F. and M.K.

Conflicts of Interest: The authors declare that they have no conflict of interest.

Availability of data and material: Experimental data is available upon request to the authors.

Code availability: R code for statistical analysis and figure creation is available upon request.

Authors' contributions: Conceptualization: H.N., M.K. and S.F. Methodology: H.N. and M.K. Formal analysis and investigation: all authors. Writing – original draft preparation: H.N.

Writing – review and editing: all authors. Funding acquisition: M.K., S.F. and H.N. Resources: M.K., S.F., and H.N. Supervision: S.F.

References

Allison SD, LeBauer DS, Ofrecio MR, et al (2009) Low levels of nitrogen addition stimulate decomposition by boreal forest fungi. Soil Biol Biochem 41:293–302. https://doi.org/10.1016/j.soilbio.2008.10.032

Almendros G, Dorado J, Sanz J, et al (1999) Compounds released by sequential chemolysis from cuticular remains of the Cretaceous Gymnosperm Squamastrobus tigrensis (Patagonia, the Argentine). Org Geochem 30:623–634. https://doi.org/10.1016/S0146-6380(99)00034-0

Arora VK, Boer GJ, Friedlingstein P, et al (2013) Carbon–Concentration and Carbon–Climate Feedbacks in CMIP5 Earth System Models. J Clim 26:5289–5314. https://doi.org/10.1175/JCLI-D-12-00494.1

Bach EM, Hofmockel KS (2015) Coupled Carbon and Nitrogen Inputs Increase Microbial Biomass and Activity in Prairie Bioenergy Systems. Ecosystems 18:417–427. https://doi.org/10.1007/s10021-014-9835-8

Baldock JA, Oades JM, Nelson PN, et al (1997) Assessing the extent of decomposition of natural organic materials using solid-state 13C NMR spectroscopy. Soil Res 35:1061–1084. https://doi.org/10.1071/s97004

Bhattacharyya A, Campbell AN, Tfaily MM, et al (2018) Redox fluctuations control the coupled cycling of iron and carbon in tropical forest soils. https://doi.org/10.1101/312108

Boye K, Noël V, Tfaily MM, et al (2017) Thermodynamically controlled preservation of organic carbon in floodplains. Nat Geosci 10:415–419. https://doi.org/10.1038/ngeo2940

Brady NC, Weil RR (2008) The nature and properties of soils. Prentice Hall, Upper Saddle River, NJ

Canfield DE, Stewart FJ, Thamdrup B, et al (2010) A Cryptic Sulfur Cycle in Oxygen-Minimum–Zone Waters off the Chilean Coast. Science 330:1375–1378. https://doi.org/10.1126/science.1196889

Canfield DE, Thamdrup B, Hansen JW (1993) The anaerobic degradation of organic matter in Danish coastal sediments: Iron reduction, manganese reduction, and sulfate reduction. Geochim Cosmochim Acta 57:3867–3883. https://doi.org/10.1016/0016-7037(93)90340-3

766 Cocozza C, D'Orazio V, Miano TM, Shotyk W (2003) Characterization of solid and aqueous
767 phases of a peat bog profile using molecular fluorescence spectroscopy, ESR and FT-IR,
768 and comparison with physical properties. Org Geochem 34:49–60.
769 https://doi.org/10.1016/S0146-6380(02)00208-5

770 Coleman DC (1994) The microbial loop concept as used in terrestrial soil ecology studies.
771 Microb Ecol 28:245–250. https://doi.org/10.1007/BF00166814

772 Coward EK, Ohno T, Sparks DL (2019) Direct Evidence for Temporal Molecular Fractionation
773 of Dissolved Organic Matter at the Iron Oxyhydroxide Interface. Environ Sci Technol
774 53:642–650. https://doi.org/10.1021/acs.est.8b04687

775 Cragg SM, Beckham GT, Bruce NC, et al (2015) Lignocellulose degradation mechanisms across
776 the Tree of Life. Curr Opin Chem Biol 29:108–119.
777 https://doi.org/10.1016/j.cbpa.2015.10.018

778 Crowther TW, Todd-Brown KEO, Rowe CW, et al (2016) Quantifying global soil carbon losses
779 in response to warming. Nature 540:104–108. https://doi.org/10.1038/nature20150

780 Davidson EA, Samanta S, Caramori SS, Savage K (2012) The Dual Arrhenius and Michaelis-
781 Menten kinetics model for decomposition of soil organic matter at hourly to seasonal
782 time scales. Glob Change Biol 18:371–384. https://doi.org/10.1111/j.1365-
783 2486.2011.02546.x

784 Dittmar T, Koch B, Hertkorn N, Kattner G (2008) A simple and efficient method for the solid-
785 phase extraction of dissolved organic matter (SPE-DOM) from seawater. Limnol
786 Oceanogr Methods 6:230–235. https://doi.org/10.4319/lom.2008.6.230

787 Doetterl S, Stevens A, Six J, et al (2015) Soil carbon storage controlled by interactions between
788 geochemistry and climate. Nat Geosci 8:780–783. https://doi.org/10.1038/ngeo2516

789 Ellis EC (2011) Anthropogenic transformation of the terrestrial biosphere. Philos Trans Math
790 Phys Eng Sci 369:1010–1035

791 Falloon P, Jones CD, Cerri CE, et al (2007) Climate change and its impact on soil and vegetation
792 carbon storage in Kenya, Jordan, India and Brazil. Agric Ecosyst Environ 122:114–124.
793 https://doi.org/10.1016/j.agee.2007.01.013

794 Fenner N, Freeman C (2011) Drought-induced carbon loss in peatlands. Nat Geosci 4:895–900.
795 https://doi.org/10.1038/ngeo1323

796 Fierer N, Allen AS, Schimel JP, Holden PA (2003) Controls on microbial CO2 production: a
797 comparison of surface and subsurface soil horizons. Glob Change Biol 9:1322–1332.
798 https://doi.org/10.1046/j.1365-2486.2003.00663.x

799 Freeman C, Ostle N, Kang H (2001) An enzymic "latch" on a global carbon store. Nature
800 409:149–149. https://doi.org/10.1038/35051650

Freeman C, Ostle NJ, Fenner N, Kang H (2004) A regulatory role for phenol oxidase during decomposition in peatlands. Soil Biol Biochem 36:1663–1667. https://doi.org/10.1016/j.soilbio.2004.07.012

Gillespie AW, Phillips CL, Dynes JJ, et al (2015) Chapter One - Advances in Using Soft X-Ray Spectroscopy for Measurement of Soil Biogeochemical Processes. In: Sparks DL (ed) Advances in Agronomy. Academic Press, pp 1–32

Grabb KC, Buchwald C, Hansel CM, Wankel SD (2017) A dual nitrite isotopic investigation of chemodenitrification by mineral-associated Fe(II) and its production of nitrous oxide. Geochim Cosmochim Acta 196:388–402. https://doi.org/10.1016/j.gca.2016.10.026

Groenigen KJ van, Qi X, Osenberg CW, et al (2014) Faster Decomposition Under Increased Atmospheric CO2 Limits Soil Carbon Storage. Science 344:508–509. https://doi.org/10.1126/science.1249534

Hall SJ, McDowell WH, Silver WL (2013) When Wet Gets Wetter: Decoupling of Moisture, Redox Biogeochemistry, and Greenhouse Gas Fluxes in a Humid Tropical Forest Soil. Ecosystems 16:576–589. https://doi.org/10.1007/s10021-012-9631-2

Hall SJ, McNicol G, Natake T, Silver WL (2015) Large fluxes and rapid turnover of mineral-associated carbon across topographic gradients in a humid tropical forest: insights from paired ^{14}C analysis. Biogeosciences 12:2471–2487. https://doi.org/10.5194/bg-12-2471-2015

Hall SJ, Treffkorn J, Silver WL (2014) Breaking the enzymatic latch: impacts of reducing conditions on hydrolytic enzyme activity in tropical forest soils. Ecology 95:2964–2973. https://doi.org/10.1890/13-2151.1

Hansel CM, Lentini CJ, Tang Y, et al (2015) Dominance of sulfur-fueled iron oxide reduction in low-sulfate freshwater sediments. ISME J 9:2400–2412. https://doi.org/10.1038/ismej.2015.50

Hedges JI, Keil RG (1995) Sedimentary organic matter preservation: an assessment and speculative synthesis. Mar Chem 49:81–115. https://doi.org/10.1016/0304-4203(95)00008-F

Hemingway JD, Rothman DH, Grant KE, et al (2019) Mineral protection regulates long-term global preservation of natural organic carbon. Nature 570:228. https://doi.org/10.1038/s41586-019-1280-6

Hodgkins SB, Richardson CJ, Dommain R, et al (2018) Tropical peatland carbon storage linked to global latitudinal trends in peat recalcitrance. Nat Commun 9:3640. https://doi.org/10.1038/s41467-018-06050-2

Huang W, Ye C, Hockaday WC, Hall SJ (2020) Trade-offs in soil carbon protection mechanisms under aerobic and anaerobic conditions. Glob Change Biol 26:3726–3737. https://doi.org/10.1111/gcb.15100

838 Jackson RB, Lajtha K, Crow SE, et al (2017) The Ecology of Soil Carbon: Pools, Vulnerabilities,
839 and Biotic and Abiotic Controls. Annu Rev Ecol Evol Syst 48:419–445.
840 https://doi.org/10.1146/annurev-ecolsys-112414-054234

841 Jakobsen R, Postma D (1999) Redox zoning, rates of sulfate reduction and interactions with Fe-
842 reduction and methanogenesis in a shallow sandy aquifer, Rømø, Denmark. Geochim
843 Cosmochim Acta 63:137–151. https://doi.org/10.1016/S0016-7037(98)00272-5

844 Jin Q, Bethke CM (2003) A New Rate Law Describing Microbial Respiration. Appl Environ
845 Microbiol 69:2340–2348. https://doi.org/10.1128/AEM.69.4.2340-2348.2003

846 Jin Q, Bethke CM (2005) Predicting the rate of microbial respiration in geochemical
847 environments. Geochim Cosmochim Acta 69:1133–1143.
848 https://doi.org/10.1016/j.gca.2004.08.010

849 Jones ME, Nico PS, Ying S, et al (2018) Manganese-Driven Carbon Oxidation at Oxic–Anoxic
850 Interfaces. Environ Sci Technol 52:12349–12357.
851 https://doi.org/10.1021/acs.est.8b03791

852 Kalbitz K, Schwesig D, Rethemeyer J, Matzner E (2005) Stabilization of dissolved organic
853 matter by sorption to the mineral soil. Soil Biol Biochem 37:1319–1331.
854 https://doi.org/10.1016/j.soilbio.2004.11.028

855 Keeler BL, Hobbie SE, Kellogg LE (2009) Effects of Long-Term Nitrogen Addition on
856 Microbial Enzyme Activity in Eight Forested and Grassland Sites: Implications for Litter
857 and Soil Organic Matter Decomposition. Ecosystems 12:1–15.
858 https://doi.org/10.1007/s10021-008-9199-z

859 Keiluweit M, Nico PS, Kleber M, Fendorf S (2016) Are oxygen limitations under recognized
860 regulators of organic carbon turnover in upland soils? Biogeochemistry 127:157–171.
861 https://doi.org/10.1007/s10533-015-0180-6

862 Keiluweit M, Wanzek T, Kleber M, et al (2017) Anaerobic microsites have an unaccounted role
863 in soil carbon stabilization. Nat Commun 8:. https://doi.org/10.1038/s41467-017-01406-6

864 Kleber M (2010) What is recalcitrant soil organic matter? Environ Chem 7:320–332.
865 https://doi.org/10.1071/EN10006

866 Koretsky CM, Moore CM, Lowe KL, et al (2003) Seasonal Oscillation of Microbial Iron and
867 Sulfate Reduction in Saltmarsh Sediments (Sapelo Island, GA, USA). Biogeochemistry
868 64:179–203

869 LaRowe DE, Dale AW, Amend JP, Van Cappellen P (2012) Thermodynamic limitations on
870 microbially catalyzed reaction rates. Geochim Cosmochim Acta 90:96–109.
871 https://doi.org/10.1016/j.gca.2012.05.011

LaRowe DE, Van Cappellen P (2011) Degradation of natural organic matter: A thermodynamic analysis. Geochim Cosmochim Acta 75:2030–2042. https://doi.org/10.1016/j.gca.2011.01.020

Lehmann J, Kleber M (2015) The contentious nature of soil organic matter. Nature. https://doi.org/10.1038/nature16069

Leifeld J, Steffens M, Galego-Sala A (2012) Sensitivity of peatland carbon loss to organic matter quality. Geophys Res Lett 39:. https://doi.org/10.1029/2012GL051856

Lichtfouse É, Chenu C, Baudin F, et al (1998) A novel pathway of soil organic matter formation by selective preservation of resistant straight-chain biopolymers: chemical and isotope evidence. Org Geochem 28:411–415. https://doi.org/10.1016/S0146-6380(98)00005-9

Lorenz K, Lal R, Preston CM, Nierop KGJ (2007) Strengthening the soil organic carbon pool by increasing contributions from recalcitrant aliphatic bio(macro)molecules. Geoderma 142:1–10. https://doi.org/10.1016/j.geoderma.2007.07.013

Lovley DR, Phillips EJP (1988) Novel Mode of Microbial Energy Metabolism: Organic Carbon Oxidation Coupled to Dissimilatory Reduction of Iron or Manganese. Appl Environ Microbiol 54:1472–1480

Luo Y, Keenan TF, Smith M (2015) Predictability of the terrestrial carbon cycle. Glob Change Biol 21:1737–1751. https://doi.org/10.1111/gcb.12766

Lützow M v, Kögel-Knabner I, Ekschmitt K, et al (2006) Stabilization of organic matter in temperate soils: mechanisms and their relevance under different soil conditions – a review. Eur J Soil Sci 57:426–445. https://doi.org/10.1111/j.1365-2389.2006.00809.x

Mann PJ, Sobczak WV, LaRue MM, et al (2014) Evidence for key enzymatic controls on metabolism of Arctic river organic matter. Glob Change Biol 20:1089–1100. https://doi.org/10.1111/gcb.12416

Marschner B, Kalbitz K (2003) Controls of bioavailability and biodegradability of dissolved organic matter in soils. Geoderma 113:211–235. https://doi.org/10.1016/S0016-7061(02)00362-2

McLatchey GP, Reddy KR (1998) Regulation of Organic Matter Decomposition and Nutrient Release in a Wetland Soil. J Environ Qual 27:1268–1274. https://doi.org/10.2134/jeq1998.00472425002700050036x

Meckenstock RU, Safinowski M, Griebler C (2004) Anaerobic degradation of polycyclic aromatic hydrocarbons. FEMS Microbiol Ecol 49:27–36. https://doi.org/10.1016/j.femsec.2004.02.019

Mokhayeri Y, Nichols A, Murthy S, et al (2006) Examining the influence of substrates and temperature on maximum specific growth rate of denitrifiers. Water Sci Technol 54:155–162. https://doi.org/10.2166/wst.2006.854

908 Nealson KH, Myers CR (1992) Microbial reduction of manganese and iron: new approaches to
909 carbon cycling. Appl Environ Microbiol 58:439–443.
910 https://doi.org/10.1128/AEM.58.2.439-443.1992

911 Pisani O, Hills KM, Courtier-Murias D, et al (2014) Accumulation of aliphatic compounds in
912 soil with increasing mean annual temperature. Org Geochem 76:118–127.
913 https://doi.org/10.1016/j.orggeochem.2014.07.009

914 Pollegioni L, Tonin F, Rosini E (2015) Lignin-degrading enzymes. FEBS J 282:1190–1213.
915 https://doi.org/10.1111/febs.13224

916 Postma D, Jakobsen R (1996) Redox zonation: Equilibrium constraints on the Fe(III)/SO4-
917 reduction interface. Geochim Cosmochim Acta 60:3169–3175.
918 https://doi.org/10.1016/0016-7037(96)00156-1

919 Poulton SW (2003) Sulfide oxidation and iron dissolution kinetics during the reaction of
920 dissolved sulfide with ferrihydrite. Chem Geol 202:79–94.
921 https://doi.org/10.1016/S0009-2541(03)00237-7

922 Pracht LE, Tfaily MM, Ardissono RJ, Neumann RB (2018) Molecular characterization of
923 organic matter mobilized from Bangladeshi aquifer sediment: tracking carbon
924 compositional change during microbial utilization. Biogeosciences 15:1733–1747.
925 https://doi.org/10.5194/bg-15-1733-2018

926 Rabus R, Wilkes H, Behrends A, et al (2001) Anaerobic Initial Reaction of n-Alkanes in a
927 Denitrifying Bacterium: Evidence for (1-Methylpentyl)succinate as Initial Product and
928 for Involvement of an Organic Radical in n-Hexane Metabolism. J Bacteriol 183:1707–
929 1715. https://doi.org/10.1128/JB.183.5.1707-1715.2001

930 Regier T, Krochak J, Sham TK, et al (2007) Performance and capabilities of the Canadian
931 Dragon: The SGM beamline at the Canadian Light Source. Nucl Instrum Methods Phys
932 Res Sect Accel Spectrometers Detect Assoc Equip 582:93–95.
933 https://doi.org/10.1016/j.nima.2007.08.071

934 RStudio Team (2016) RStudio: Integrated Development for R. RStudio, Inc., Boston, MA

935 Schink B (2002) Anaerobic digestion: concepts, limits and perspectives. Water Sci Technol
936 45:1–8. https://doi.org/10.2166/wst.2002.0274

937 Schink B (1985) Degradation of unsaturated hydrocarbons by methanogenic enrichment cultures.
938 FEMS Microbiol Lett 31:69–77. https://doi.org/10.1111/j.1574-6968.1985.tb01133.x

939 Schink B, Philipp B, Müller JA (2000) Anaerobic degradation of phenolic compounds.
940 Naturwissenschaften 87:12–23

941 Schmidt MW (2012) Persistence of soil organic matter as an ecosystem property. Nat 478 49-56.
942 https://doi.org/DOI: 10.1038/nature10386

Sengupta A, Indivero J, Gunn C, et al (2019) Spatial gradients in the characteristics of soil-carbon fractions are associated with abiotic features but not microbial communities. Biogeosciences 16:3911–3928. https://doi.org/10.5194/bg-16-3911-2019

Sexstone AJ, Revsbech NP, Parkin TB, Tiedje JM (1985) Direct Measurement of Oxygen Profiles and Denitrification Rates in Soil Aggregates1. Soil Sci Soc Am J 49:645. https://doi.org/10.2136/sssaj1985.03615995004900030024x

Sinsabaugh RL (2010) Phenol oxidase, peroxidase and organic matter dynamics of soil. Soil Biol Biochem 42:391–404. https://doi.org/10.1016/j.soilbio.2009.10.014

Sinsabaugh RL, Gallo ME, Lauber C, et al (2005) Extracellular Enzyme Activities and Soil Organic Matter Dynamics for Northern Hardwood Forests receiving Simulated Nitrogen Deposition. Biogeochemistry 75:201–215. https://doi.org/10.1007/s10533-004-7112-1

So CM, Young LY (1999) Initial Reactions in Anaerobic Alkane Degradation by a Sulfate Reducer, Strain AK-01. Appl Environ Microbiol 65:5532–5540. https://doi.org/10.1128/AEM.65.12.5532-5540.1999

Sokol NW, Sanderman J, Bradford MA (2019) Pathways of mineral-associated soil organic matter formation: Integrating the role of plant carbon source, chemistry, and point of entry. Glob Change Biol 25:12–24. https://doi.org/10.1111/gcb.14482

Sollins P, Homann P, Caldwell BA (1996) Stabilization and destabilization of soil organic matter: mechanisms and controls. Geoderma 74:65–105. https://doi.org/10.1016/S0016-7061(96)00036-5

Sørensen J (1982) Reduction of Ferric Iron in Anaerobic, Marine Sediment and Interaction with Reduction of Nitrate and Sulfate. Appl Environ Microbiol 43:319–324. https://doi.org/10.1128/AEM.43.2.319-324.1982

Stegen JC, Johnson T, Fredrickson JK, et al (2018) Influences of organic carbon speciation on hyporheic corridor biogeochemistry and microbial ecology. Nat Commun 9:585. https://doi.org/10.1038/s41467-018-02922-9

Stookey LL (1970) Ferrozine---a new spectrophotometric reagent for iron. Anal Chem 42:779–781. https://doi.org/10.1021/ac60289a016

Stuckey JW, Schaefer MV, Kocar BD, et al (2016) Arsenic release metabolically limited to permanently water-saturated soil in Mekong Delta. Nat Geosci 9:70–76. https://doi.org/10.1038/ngeo2589

Thamdrup B (2000) Bacterial Manganese and Iron Reduction in Aquatic Sediments. In: Schink B (ed) Advances in Microbial Ecology. Springer US, Boston, MA, pp 41–84

Tiedje JM (1988) Ecology of denitrification and dissimilatory nitrate reduction to ammonium. In: Biology of anaerobic microorganisms. pp 179–244

Tolić N, Liu Y, Liyu A, et al (2017) Formularity: Software for Automated Formula Assignment of Natural and Other Organic Matter from Ultrahigh-Resolution Mass Spectra. Anal Chem 89:12659–12665. https://doi.org/10.1021/acs.analchem.7b03318

Torn MS, Trumbore SE, Chadwick OA, et al (1997) Mineral control of soil organic carbon storage and turnover. Nature 389:170–173. https://doi.org/10.1038/38260

Warneke S, Schipper LA, Matiasek MG, et al (2011) Nitrate removal, communities of denitrifiers and adverse effects in different carbon substrates for use in denitrification beds. Water Res 45:5463–5475. https://doi.org/10.1016/j.watres.2011.08.007

Wieder WR, Bonan GB, Allison SD (2013) Global soil carbon projections are improved by modelling microbial processes. Nat Clim Change 3:909–912. https://doi.org/10.1038/nclimate1951

Wilpiszeski RL, Aufrecht JA, Retterer ST, et al (2019) Soil Aggregate Microbial Communities: Towards Understanding Microbiome Interactions at Biologically Relevant Scales. Appl Environ Microbiol 85:e00324-19. https://doi.org/10.1128/AEM.00324-19

Ying SC, Masue-Slowey Y, Kocar BD, et al (2013) Distributed microbially- and chemically-mediated redox processes controlling arsenic dynamics within Mn-/Fe-oxide constructed aggregates. Geochim Cosmochim Acta 104:29–41. https://doi.org/10.1016/j.gca.2012.08.020

Zhou J, Xue K, Xie J, et al (2012) Microbial mediation of carbon-cycle feedbacks to climate warming. Nat Clim Change 2:106–110. https://doi.org/10.1038/nclimate1331

Figure 1 Cumulative total inorganic carbon production, including effluent dissolved inorganic carbon and headspace carbon dioxide (a), and cumulative dissolved organic carbon production (b). Means and standard error across reactors for a given treatment are displayed

Figure 2 Depth profiles of porewater redox indicators at the final sampling timepoint, including nitrate (a), nitrite (b), sulfate (c) and porewater iron, which was assumed to be Fe(II) (d). Non-metal species show the mean and standard error between replicate reactors, whereas iron shows mean and standard error of duplicate Ferrozine assays performed on replicate reactors

Figure 3 0.5 M HCl-extractable manganese (a) and iron (b) measured on six depth increments sampled post-experiment. Standard error bars capture error around the mean of duplicate measurements for each reactor

Figure 4 Depth profiles of dissolved organic carbon (a), dissolved inorganic carbon (b), carbon dioxide produced after overnight anaerobic incubations of soils (30 h; c), and average nominal oxidation state of organic matter (NOSC) of porewater DOC (d). Porewater samples were collected the day prior to solid sampling and anaerobic incubations. All values in panels a-c

represent the mean and standard error across treatment replicates with incubations additionally run in duplicate; 95% confidence interval around the mean is displayed for NOSC data

Fig. 5 Thermodynamic potential factor (a) and Gibbs free energy of reaction (b) modeled as a function of nominal oxidation state of carbon (NOSC) as detailed in the Electronic Supplementary Material using measured geochemical data. CON reactors are represented by oxic respiration at the surface and ferric iron (ferrihydrite) reduction at depth. NIT and SULF reactors are represented by denitrification and sulfate reduction reactions, respectively, at both the surface and at depth. All redox reactions, free energy calculations and microbial physiological parameters were normalized to per-mole of carbon oxidized

Fig. 6 Correlation matrix for geochemical factors (a). The colorbar and dot size represent Spearman rank coefficient strength and direction, while the presence of a dot represents significance at $p < 0.05$. Black boxes indicate clusters of factors that group together after hierarchical tree clustering using complete linkage (b; "C" = Cluster). Organic compound or moiety relative abundances are derived from C-NEXAFS and FT-ICR-MS data; gas production values are taken from anaerobic incubations; Feratio ($Fe(II)/Fe_{total}$), FeII (Fe(II)) and Fetot (Fe_{total}) are taken from HCl extracts; SO4 (SO_4^{2-}), NO3 (NO_3^-), NO2 (NO_2^-) and poreFe (porewater Fe) are taken from rhizon samplers; and pH and DO (dissolved oxygen) are taken from microelectrode profiles. DBE = double bond equivalent, OC and HC are the average ratios of O and H atoms to C atoms in a DOC sample, CONDENS = condensed aromatics, CARBO = carbohydrates, AMINOSUG = aminosugars, UNSATHC = unsaturated hydrocarbons, and ALKYLOH = alcohols

Figure 7 Biplots of the first and second principal components in principal component analysis (PCA) showing samples coded by depth (a) and treatment (b). Arrows represent loadings and points represent sample scores, where circles encompass one standard deviation around a normal distribution for each sample grouping in biplot space. Organic functional groups are derived from C-NEXAFS data; gas production values are taken from anaerobic incubations; Feratio ($Fe(II)/Fe_{total}$), FeII (Fe(II)) and Fetot (Fe_{total}) are taken from HCl extracts; SO4 (SO_4^{2-}), NO3 (NO_3^-), NO2 (NO_2^-) and poreFe (porewater Fe) are taken from rhizon samplers; and pH and DO (dissolved oxygen) are taken from microelectrode profiles

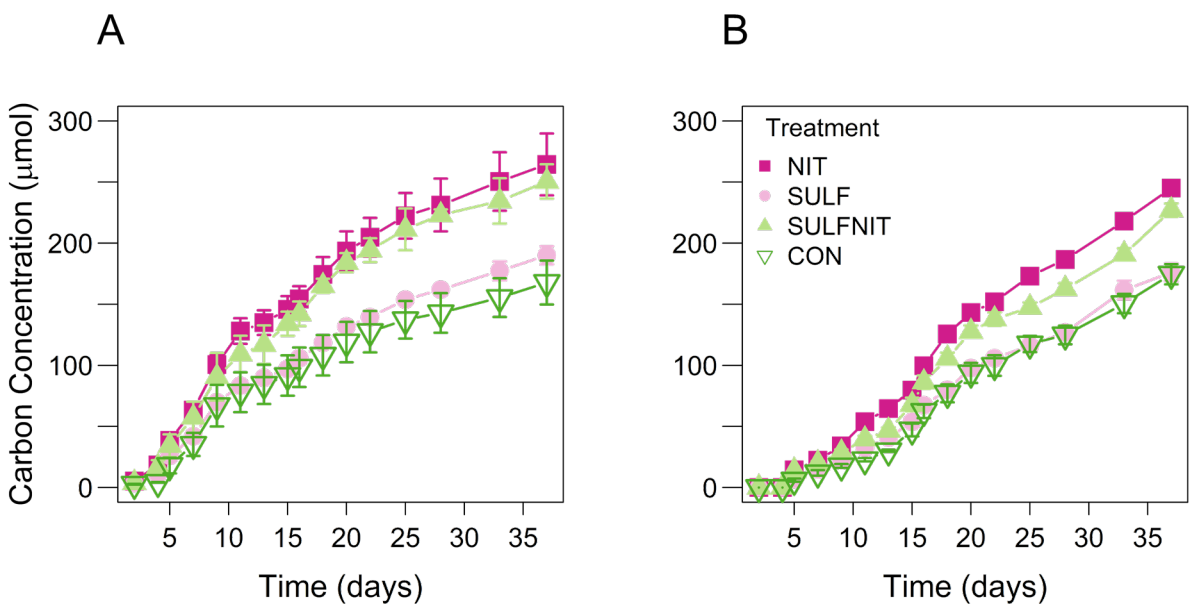
A
B
Carbon Concentration (µmol)
300
200
100
0
5
10
15
20
25
30
35
Time (days)
Treatment
NIT
SULF
SULFNIT
CON

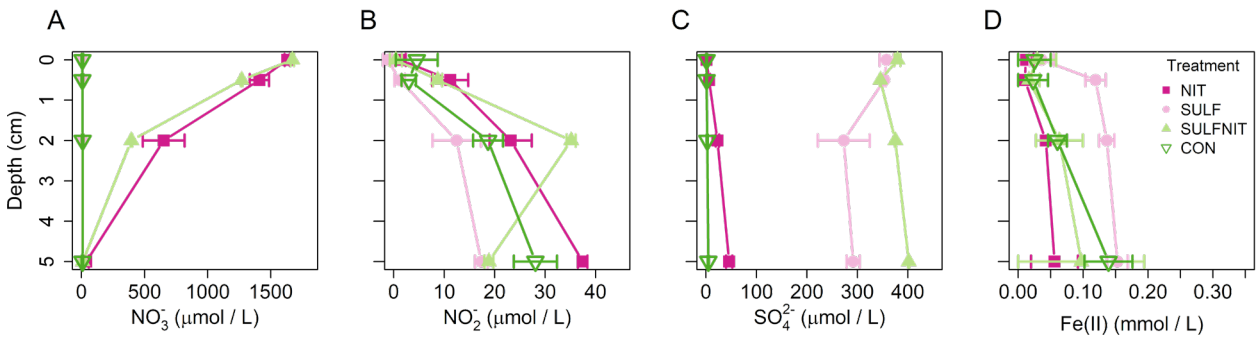
A
B
C
D
Depth (cm)
0
1
2
3
4
5
0
500
1000
1500
NO_3^- (µmol / L)
0
10
20
30
40
NO_2^- (µmol / L)
0
100
200
300
400
SO_4^{2-} (µmol / L)
0.00
0.10
0.20
0.30
Fe(II) (mmol / L)
Treatment
NIT
SULF
SULFNIT
CON

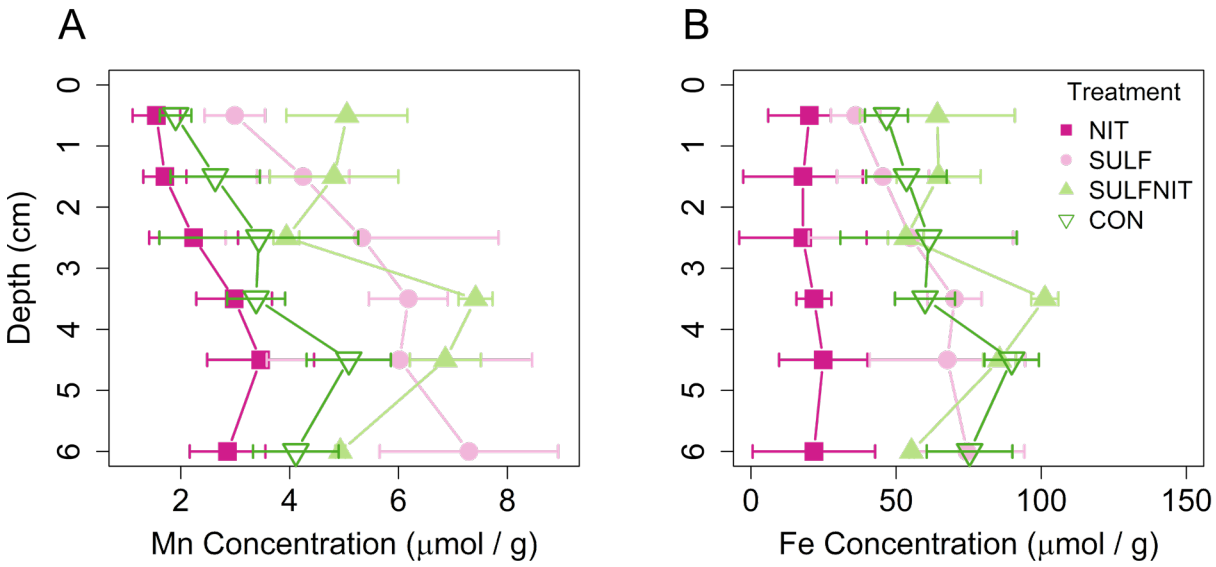
A
B
Depth (cm)
0
1
2
3
4
5
6
2
4
6
8
Mn Concentration (μmol / g)
0
50
100
150
Fe Concentration (μmol / g)
Treatment
NIT
SULF
SULFNIT
CON

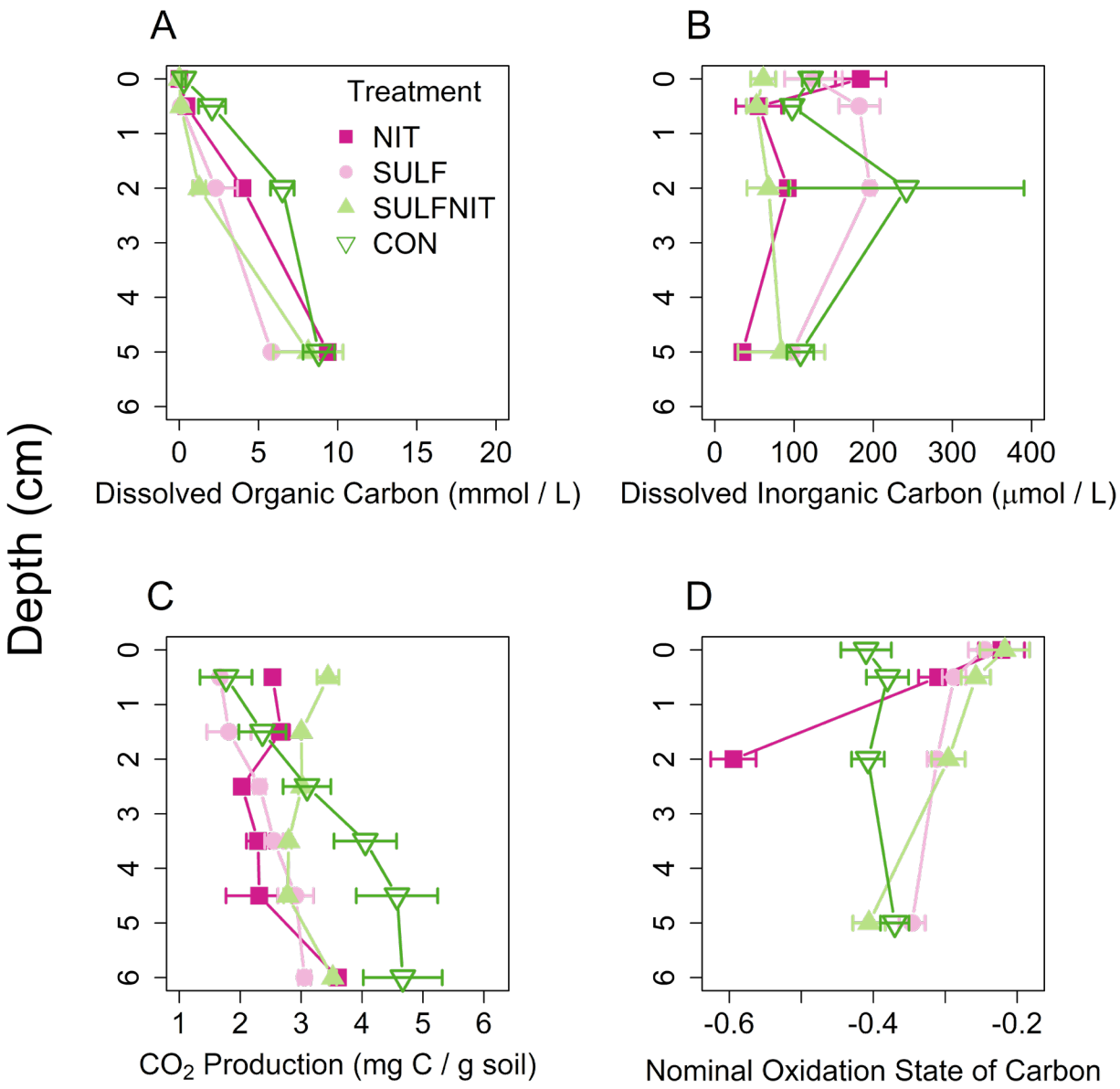
A
B
C
D
Depth (cm)
Treatment
NIT
SULF
SULFNIT
CON
Dissolved Organic Carbon (mmol / L)
Dissolved Inorganic Carbon (μmol / L)
CO2 Production (mg C / g soil)
Nominal Oxidation State of Carbon

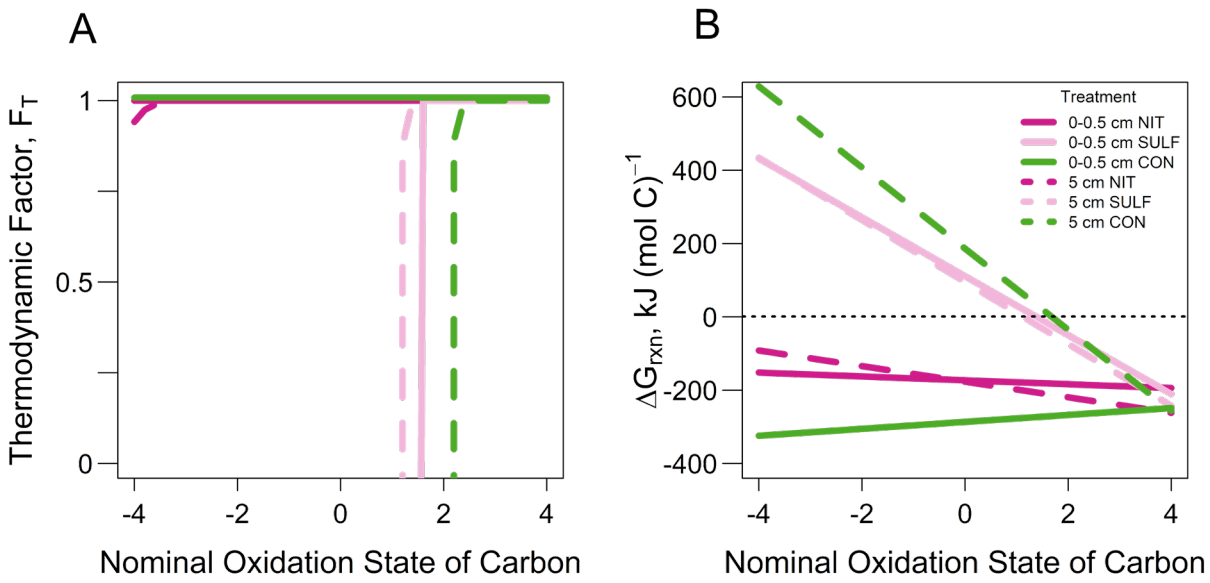
A
Thermodynamic Factor, F_T
1
0.5
0
-4
-2
0
2
4
Nominal Oxidation State of Carbon
B
ΔG_{rxn}, kJ (mol C)$^{-1}$
600
400
200
0
-200
-400
Treatment
0-0.5 cm NIT
0-0.5 cm SULF
0-0.5 cm CON
5 cm NIT
5 cm SULF
5 cm CON
-4
-2
0
2
4
Nominal Oxidation State of Carbon

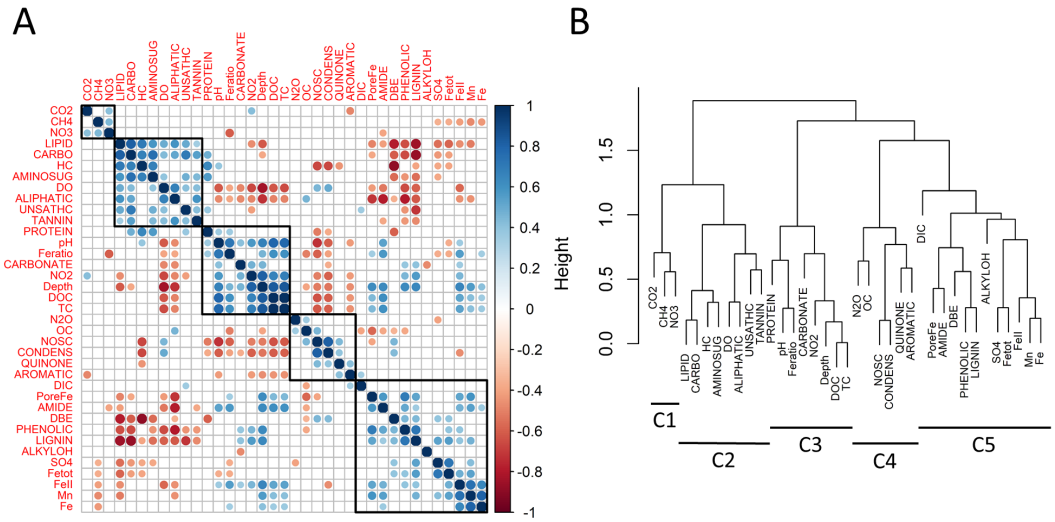
A
B
Height
1
0.8
0.6
0.4
0.2
0
-0.2
-0.4
-0.6
-0.8
-1
0.0
0.5
1.0
1.5
C1
C2
C3
C4
C5

1165

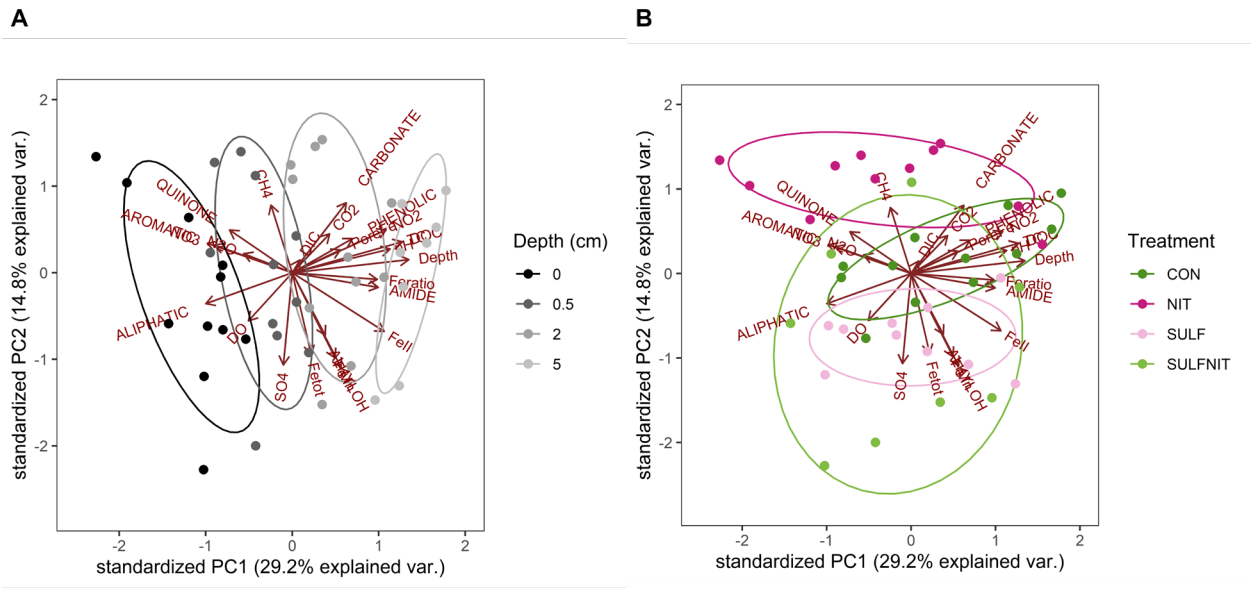
A
B
standardized PC2 (14.8% explained var.)
standardized PC1 (29.2% explained var.)
CARBONATE
QUINONE
AROMATIC
CH4
CO2
PHENOLIC
TDN
TDC
Depth
Feratio
AMIDE
ALIPHATIC
DO
Fe3
SO4
Fe1or2
Depth (cm)
0
0.5
2
5
Treatment
CON
NIT
SULF
SULFNIT

1166